Supporting Information for

Photochemical Formation and Transformation of Birnessite: Effects of Cations on Micromorphology and Crystal Structure

Tengfei Zhang,[†] Lihu Liu,[†] Wenfeng Tan,[†] Steven L. Suib,[‡] Guohong Qiu,*[,†] Fan Liu[†]

[†] Key Laboratory of Arable Land Conservation (Middle and Lower Reaches of Yangtse River), Ministry of Agriculture, Hubei Key Laboratory of Soil Environment and Pollution Remediation, College of Resources and Environment, Huazhong Agricultural University, Wuhan 430070, Hubei Province, China

[‡] Department of Chemistry, University of Connecticut, 55 North Eagleville Road, Storrs, Connecticut, 06269-3060, USA

* Corresponding author: Qiu GH, E-mail: qiugh@mail.hzau.edu.cn

SI Supporting Methods

SII Supporting Tables and Figures

22 Pages, 2 Tables and 16 Figures

SI Supporting Methods

S1. Sample Collection

The quartz tubes were brought back to the glove box after photochemical reaction. The precipitates were collected and washed with deoxygenated deionized water by filtrating through 0.22 μm microporous membrane in the glove box until the conductivity of the filtrate was below 5 μS cm^{-1}. The microporous membrane adhered by manganese oxides was then put into a 50-mL plastic centrifuge tube containing 30 mL deoxygenated deionized water. The plastic centrifuge tube was taken out from the glove box and ultrasonic dispersed for 10 s. Then, the solids were collected by centrifugation at 12000 rmp min^{-1} for 5 min. The collected wet solids were analyzed by XRD, then dried at 40 °C in a vacuum drying oven (DZF−6021, Yiheng Instrument Factory Co. Ltd., China).

S2. Oxidation of Mn^{2+}_{aq} in the Presence of SOD/BA

Superoxide dismutase (SOD) is a kind of metalloenzyme that can dismutate $O_2^{\bullet-}$ to H_2O_2 and O_2.[1,2] To confirm the role of $O_2^{\bullet-}$, Mn^{2+}_{aq} photooxidation experiments were performed in the presence of SOD (20 mg L^{-1}) with UV irradiation under anoxic and oxic conditions, respectively. Benzoate (BA) could react with $OH^{\bullet}$ to form stable and measurable product of *p*-hydroxybenzoic acid (*p*-HBA), which could be determined at 255 nm by high-performance liquid chromatography.[3,4] To clarify the effect of $OH^{\bullet}$, the experiments of Mn^{2+}_{aq} oxidation were carried out in the presence of excess BA (20 mmol L^{-1}) under anoxic and oxic conditions, respectively. The corresponding concentration of accumulated $OH^{\bullet}$ was about 6 times that of *p*-HBA.[3] In order to confirm the formation of $O_2^{\bullet-}$ from NO_2^-, the mixed solution of 0.25 mmol L^{-1} $MnSO_4$ and 10 mmol L^{-1} $NaNO_2$ with initial pH 6.0 was exposed to UV irradiation under oxic conditions.

S3. XAS Spectra Analyses

The samples of 0.01Na-HB, 0.1Na-HB, 0.1Mg-HB, and 0.1K-HB were also analyzed by the (X-ray absorption fine structure) XAFS spectra. Spectra were collected in transmission mode over the energy range of 6381–7321 eV. The monochromator energy was calibrated by a Mn metal foil (E_0 = 6539 eV). All XAS data were background-subtracted, normalized and Fourier transformed using the software Ifeffit/Athena.[5] The background removal of Mn *K*-edge spectra was performed with the following parameters: E_0 = 6539 eV, *Rbkg* = 1.0 Å, and *k*-weight = 3. All Mn *K*-edge X-ray absorption near edge structure (XANES) spectra were fitted using the Combo method to obtain the Mn average oxide state.[6] The analysis of Fourier transformed (extended X-Ray absorption fine structure) EXAFS data ($1.0 < R + \delta R < 3.5$ Å) was performed in the single-scattering approximation using the software Ifeffit/Artemis for spectral simulations.[7] The amplitude reduction factor (S_0^2) was calibrated using λ-MnO_2 and determined to be 0.73 for the O_1 shell and 0.80 for the Mn shell.[7]

SII Supporting Tables and Figures

Table S1. Fractional and average oxide state (AOS) of Mn obtained from the Combo fit of Mn *K*-edge XANES spectra of 0.01Na-HB, 0.1Na-HB, 0.1Mg-HB, and 0.1K-HB in the 6521–6653 eV interval.

Sample	Mn(II) (at.%)	Mn(III) (at.%)	Mn(IV) (at.%)	Mn AOS
0.01Na-HB	12	16	72	3.60
0.1Na-HB	15	9	76	3.61
0.1Mg-HB	16	9	75	3.59
0.1K-HB	13	9	78	3.65

Table S2. Optimized simulation parameters derived from Mn *K*-edge EXAFS.

Sample	Shells	*CN*	*Dist* (Å)	σ^2	ΔE (eV)
0.01Na-HB	Mn-O_1	4.4	1.90	0.0038	3.84
	Mn-O_2	6.0	3.57	0.0028	
	Mn-Mn_{edg}	4.3	2.89	0.0067	
	Mn-Mn_{cor}	3.7	3.44	0.0067	
0.1Na-HB	Mn-O_1	4.8	1.90	0.0039	6.05
	Mn-O_2	6.0	3.57	0.0050	
	Mn-Mn_{edg}	5.1	2.87	0.0069	
	Mn-Mn_{cor}	2.8	3.45	0.0069	
0.1Mg-HB	Mn-O_1	4.7	1.91	0.0039	5.56
	Mn-O_2	6.0	3.57	0.0099	
	Mn-Mn_{edg}	5.0	2.87	0.0070	
	Mn-Mn_{cor}	2.0	3.47	0.0070	
0.1K-HB	Mn-O_1	5.3	1.91	0.0042	5.68
	Mn-O_2	6.0	3.56	0.0023	
	Mn-Mn_{edg}	5.37	2.89	0.0065	
	Mn-Mn_{cor}	3.19	3.43	0.0065	

Note: *CN*, coordination number; *Dist*, interatomic distance; σ^2, Debye-Waller parameter; ΔE, energy shift. Fitting procedure details reference to Villalobos et al.[7] S_0^2 values used for the amplitude normalization were 0.73 for the O_1 shell and 0.80 for the Mn shells. σ^2 values for the Mn_{edg} and Mn_{cor} shells were variable but kept identical. The coordination number (*CN*) of the O_2 shells was a fixed value.

Figure. S1 Photos of PL-03 photochemical reaction instrument (Beijing Precise Technology Co., Ltd.).

As shown in Figure S1, the quartz tubes were placed around the light source, and the distance of quartz tubes from the light source was 8.3 cm. In addition, the turntable for placing quartz tubes was revolving around the light to make sure that the quartz tubes were evenly illuminated in the photochemical reaction processes.

75

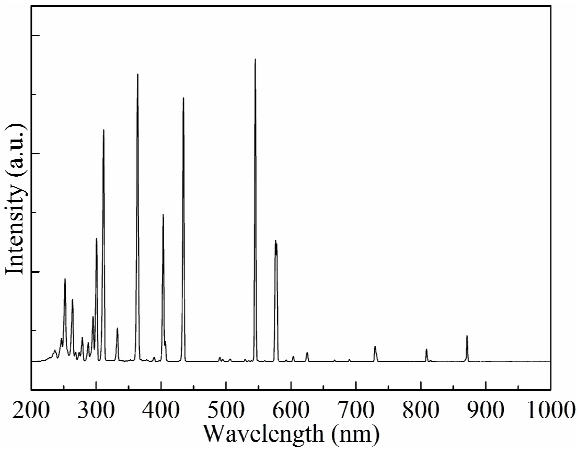

76

77 **Figure S2.** Spectral curve of the mercury lamp. The data were collected using S3000-UV-NIR

78 spectrometer by the Beijing Precise Technology Co., Ltd.

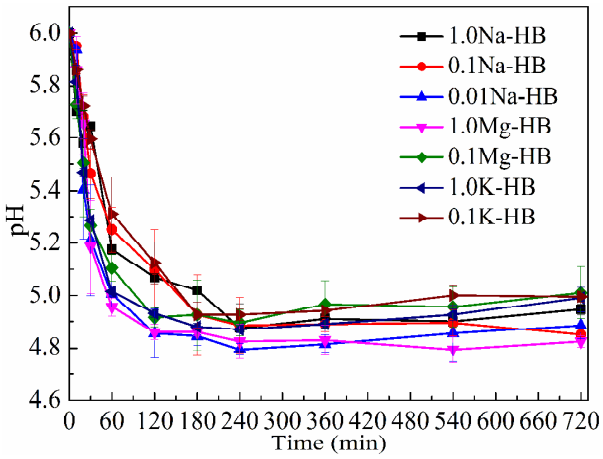

Figure S3. Changes in pH during the formation of birnessite in the presence of different cations.

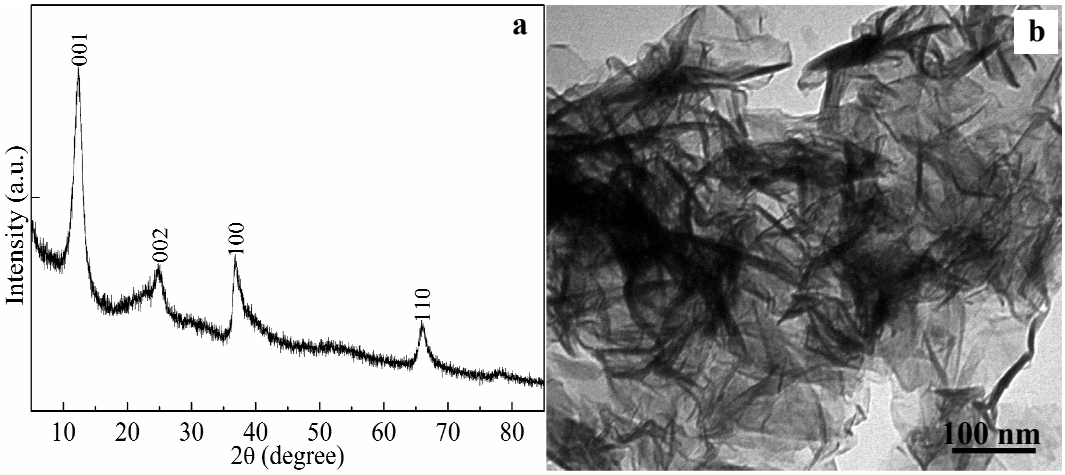

Figure S4. XRD pattern (a) and HRTEM (b) image of sample formed in a mixed aqueous solution of 0.25 mmol L^{-1} $MnSO_4$ and 10 mmol L^{-1} $NaNO_3$ with solar light irradiation for 12 h under anoxic conditions.

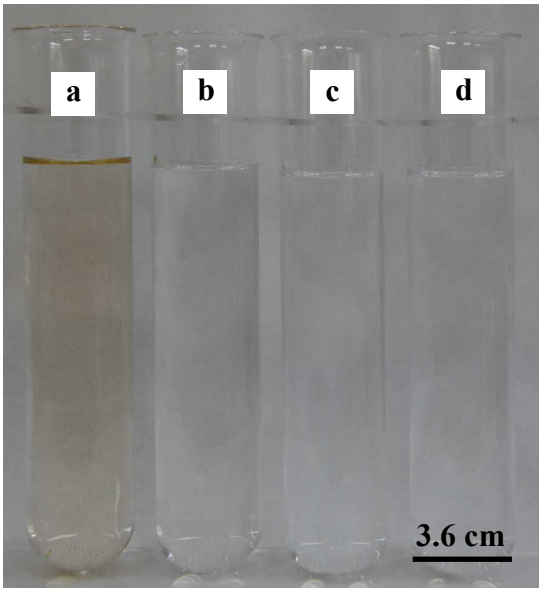

Figure S5. Photograph of the reaction system of $MnSO_4$ (0.25 mmol L^{-1}) and $NaNO_3$ (10 mmol L^{-1}) under UV (a), Vis (b) irradiation, and dark conditions (c) and the reaction system of $MnSO_4$ (0.25 mmol L^{-1}) under UV irradiation (d) under anoxic conditions for 12 h.

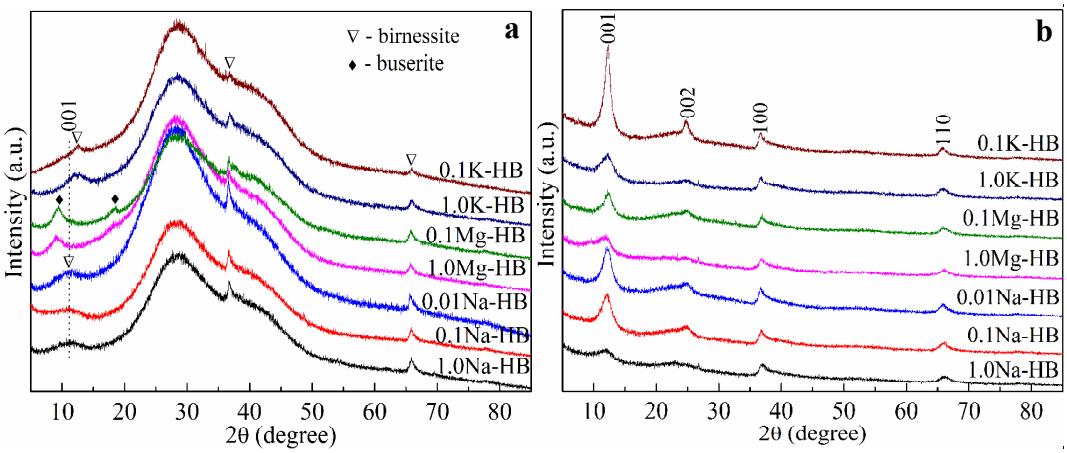

Figure S6. XRD patterns of wet pastes (a) and dried powders (b) of 1.0Na-HB, 0.1Na-HB, 0.01Na-HB, 1.0Mg-HB, 0.1Mg-HB, 1.0K-HB, and 0.1K-HB.

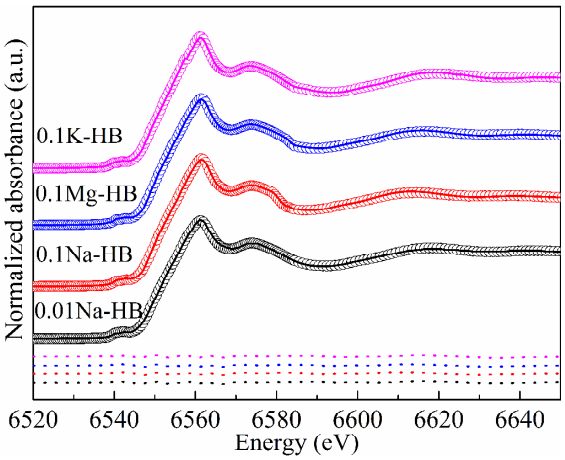

Figure S7. Normalized Mn *K*-edge XANES spectra (open circles) and best-fitted curves of 0.01Na-HB, 0.1Na-HB, 0.1Mg-HB, and 0.1K-HB using the Combo method in the 6521–6653 eV interval (difference plots are indicated at bottom).

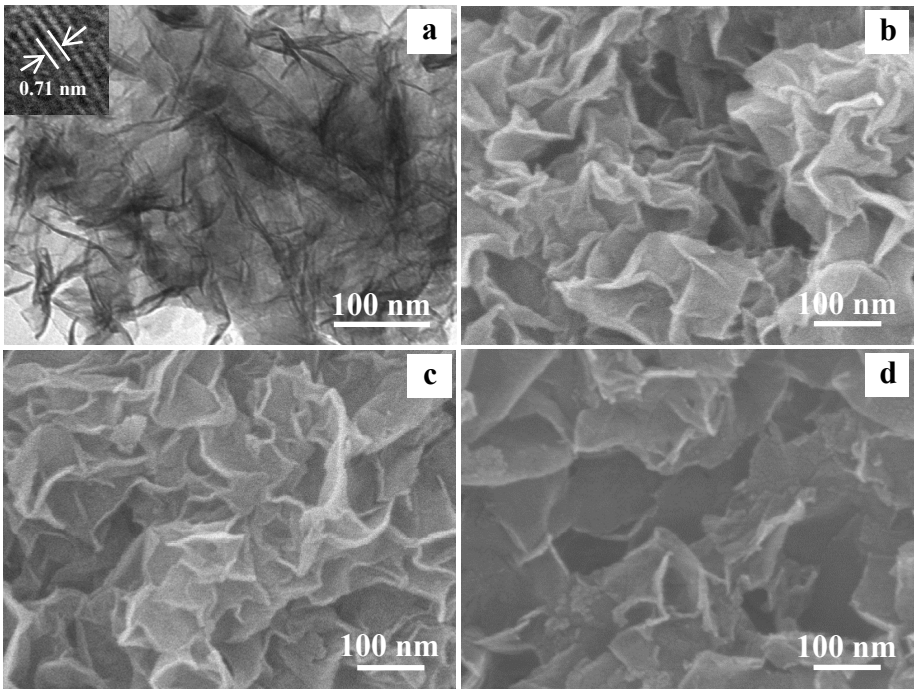

Figure S8. HRTEM and FESEM images of 0.01Na-HB (a), 1.0Na-HB (b), 1.0Mg-HB (c), and 1.0K-HB (d).

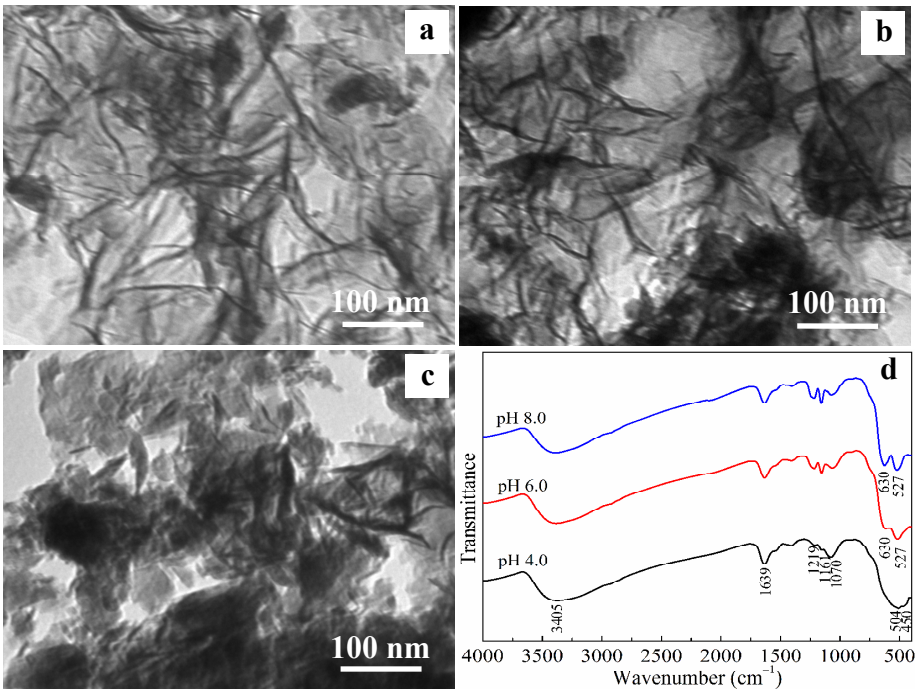

Figure S9. TEM images of transformation products of birnessite at constant pH 4.0 (a), pH 6.0 (b), and pH 8.0 (c) under oxic conditions for 30 days and the corresponding FTIR spectra (d).

Figure S9d shows the FTIR spectra of the transformation products of birnessite at constant pH 4.0, 6.0 and 8.0 for 30 days. The absorption bands at 527 and 630 cm^{-1} were owing to the Mn–O lattice vibration of hausmannite, further suggesting the formation of hausmannite in the transformation reaction of birnessite.[8]

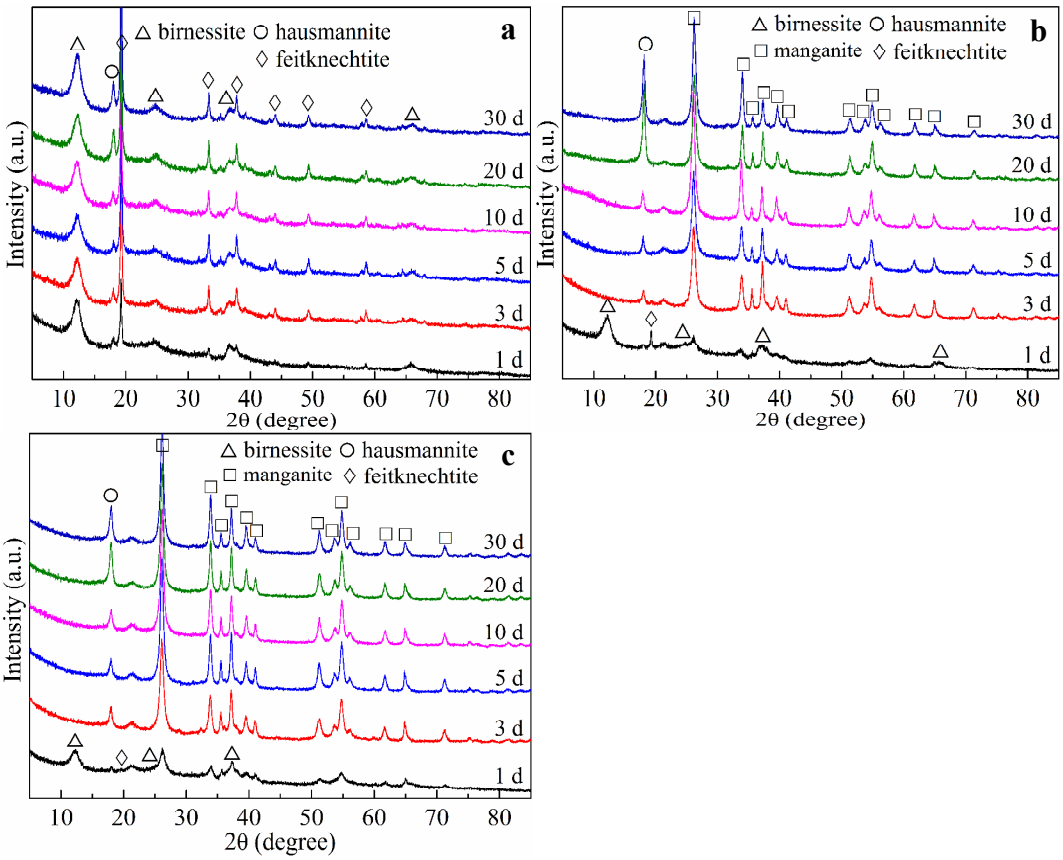

Figure S10. XRD patterns of birnessite transformation products after treatment with 0.7 (a), 3.5 (b), and 7.0 mmol L^{-1} (c) Mn^{2+}_{aq} at constant pH 8.0 for different time periods under oxic conditions.

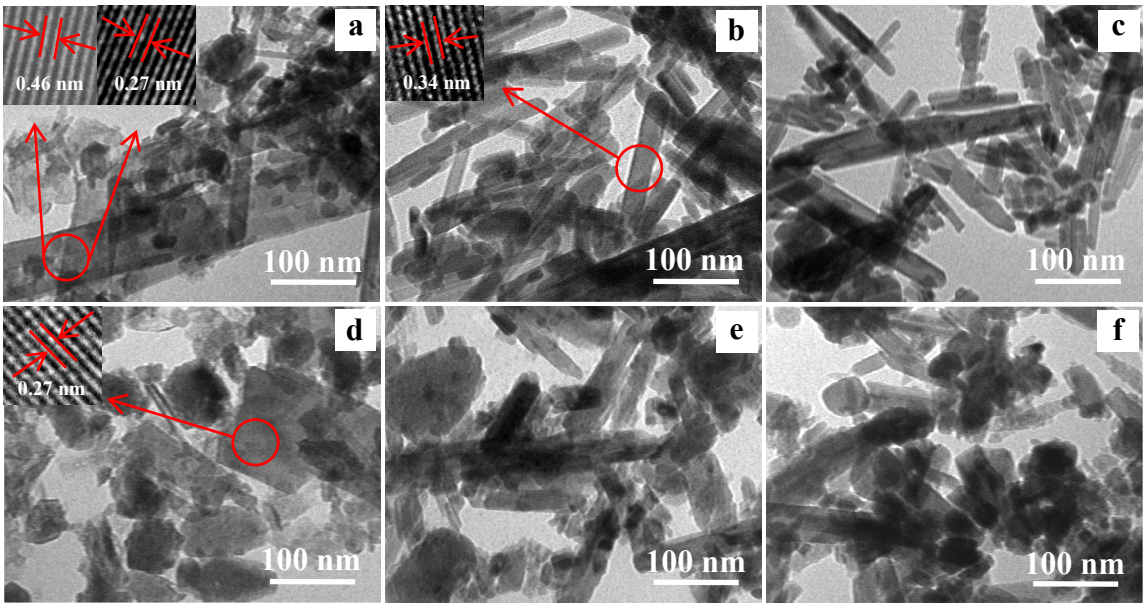

Figure S11. HRTEM images of tranformation products of birnessite after 30 days in the solutions with initial Mn^{2+}_{aq} concentrations of 0.7 (a), 3.5 (b) and 7.0 mmol L^{-1} (c) under oxic conditions, and 0.7 (d), 3.5 (e) and 7.0 mmol L^{-1} (f) at constant pH 8.0 under anoxic conditions.

HRTEM images of tranformation products of birnessite after 30 days in the solutions with various initial Mn^{2+}_{aq} concentrations at constant pH 8.0 under oxic and anoxic conditions are shown in Figure S11. The lattice fringes separated by ~0.46 and 0.27 nm respectively correspond to the (002) and (311) planes of feitknechtite (Figures S11a, d). The lattice fringes separated by ~0.34 nm correspond to the (−111) plane of manganite (Figure S11b). These results suggest that lath-shaped feitknechtite, rod-shaped manganite, and hausmannite particles are formed.

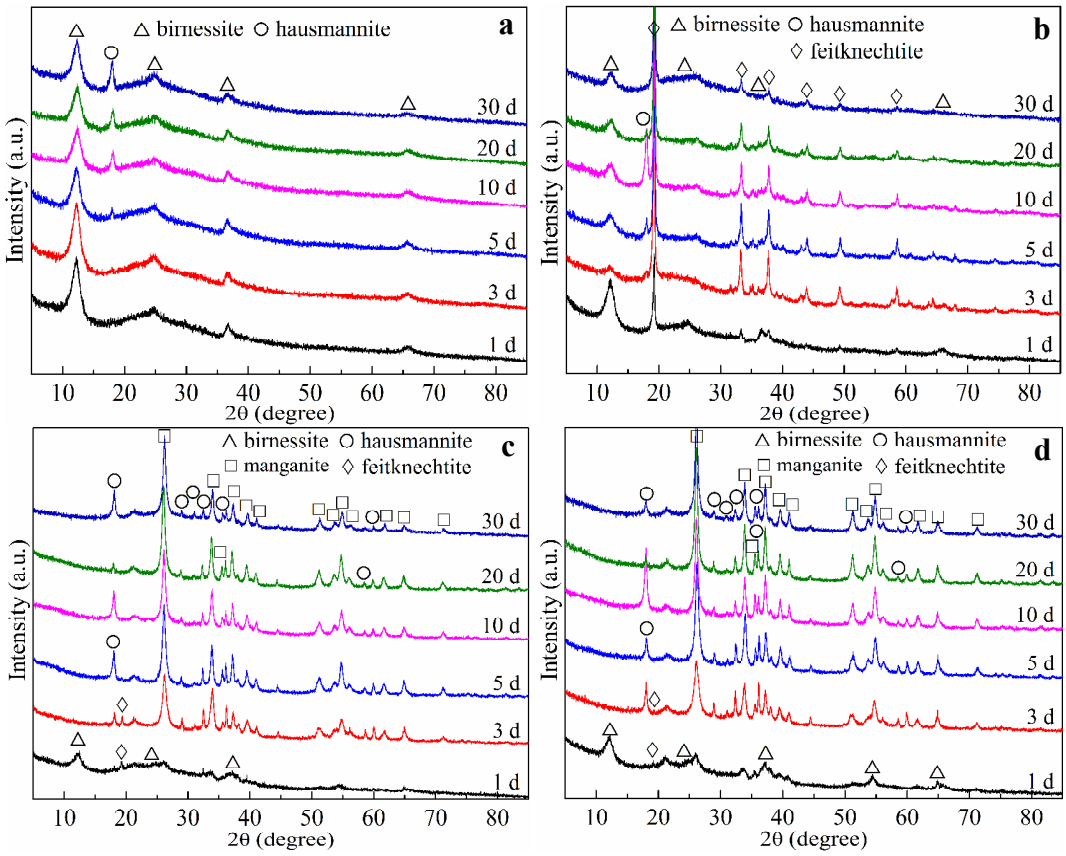

Figure S12. XRD patterns of tranformation products of birnessite after treatment with 0 (a), 0.7 (b), 3.5 (c), and 7.0 mmol L^{-1} (d) Mn^{2+}_{aq} at constant pH 8.0 for different time periods under anoxic conditions.

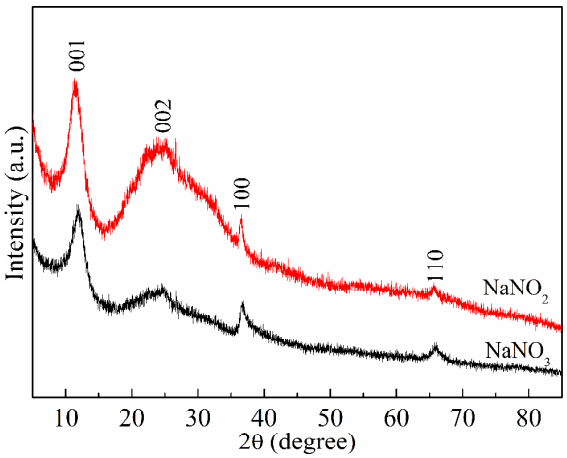

Figure S13. XRD patterns of the samples obtained through the reaction of 0.25 mmol L^{-1} $MnSO_4$ and 10 mmol L^{-1} $NaNO_2$/$NaNO_3$ with UV irradiation under oxic conditions for 12 h.

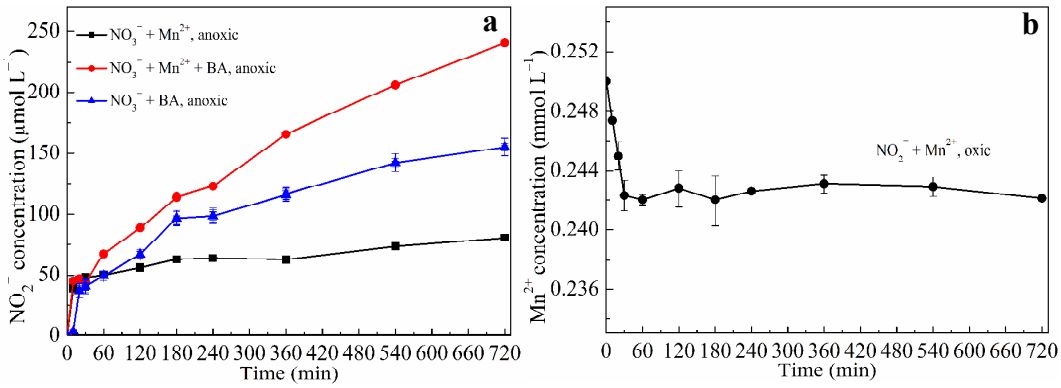

Figure S14. Concentrations of NO_2^- (a) and Mn^{2+} (b) under different conditions at initial pH 6.0 with UV irradiation.

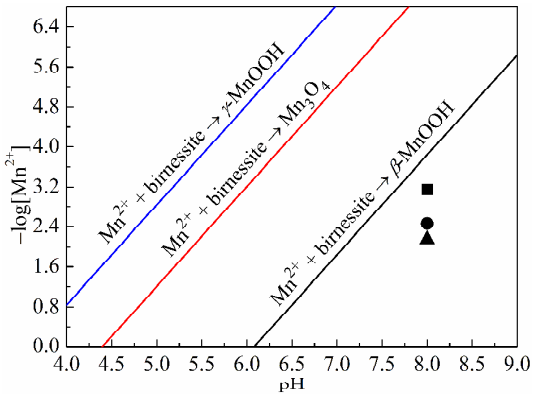

Figure S15. Logarithm of Mn^{2+} concentration ($\log[Mn^{2+}]$) versus pH critical lines determined by three different reactions: Mn^{2+}-birnessite equilibrium with manganite (γ-MnOOH), hausmannite (Mn_3O_4) and feitknechtite (β-MnOOH), calculated based on thermodynamic data provided by Hem et al.[9] (■, ● and ▲ represent the reaction of 0.7, 3.5 and 7.0 mmol L^{-1} Mn^{2+} and photosynthesized birnessite at constant pH 8.0, respectively)

The relationship between pH and Mn^{2+}_{aq} concentration ($[Mn^{2+}]$) was calculated based on the reaction isotherm $\Delta_r G_m^{\,o} = -RT\ln k_{eq}$,[10,11] where $\Delta_r G_m^{\,o}$ is obtained from the standard Gibbs free energies of the product and reactant species ($\Delta_r G_m^{\,o} = \Sigma(\Delta_f G_m^{\,o})_{products} - \Sigma(\Delta_f G_m^{\,o})_{reactants}$), k_{eq} is equilibrium constant, R is molar gas constant (R = 8.314 J mol^{-1} K^{-1}), and T is 273 K. The relationship between pH and $[Mn^{2+}]$: feitknechtite: $-\log[Mn^{2+}] = 2pH - 12.16$; hausmannite: $-\log[Mn^{2+}] = 2pH - 8.79$; and manganite: $-\log[Mn^{2+}] = 2pH - 7.16$. This graph could be used to estimate the thermodynamical possibility for a reaction.

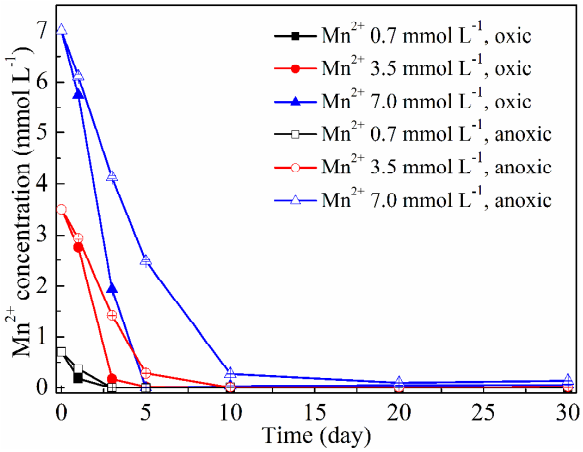

Figure S16. Concentration changes of Mn^{2+}_{aq} in the transformation of birnessite with 0.7–7.0 mmol L^{-1} Mn^{2+}_{aq} at different time periods under oxic and anoxic conditions.

Supporting References

(1) Riley, D. P. Functional mimics of superoxide dismutase enzymes as therapeutic agents. *Chem. Rev.* **1999**, *99* (9), 2573–2588.

(2) Ryu, J.; Choi, W. Effects of TiO_2 surface modifications on photocatalytic oxidation of arsenite: the role of superoxides. *Environ. Sci. Technol.* **2004**, *38* (10), 2928–2933.

(3) Zhang, P.; Yuan, S. H.; Liao, P. Mechanisms of hydroxyl radical production from abiotic oxidation of pyrite under acidic conditions. *Geochim. Cosmochim. Acta* **2016**, *172*, 444–457.

(4) Joo, S. H.; Feitz, A. J.; Sedlak, D. L.; Waite, T. D. Quantification of the oxidizing capacity of nanoparticulate zero-valent iron. *Environ. Sci. Technol.* **2005**, *39* (5), 1263–1268.

(5) Webb, S. M. SIXpack: a graphical user interface for XAS analysis using IFEFFIT. *Phys. Scr.* **2005**, *T115*, 1011.

(6) Manceau, A.; Marcus, M. A.; Grangeon, S. Determination of Mn valence states in mixed-valent manganates by XANES spectroscopy. *Am. Mineral.* **2012**, *97* (5–6), 816–827.

(7) Villalobos, M.; Lanson, B.; Manceau, A.; Toner, B.; Sposito, G. Structural model for the biogenic Mn oxide produced by *Pseudomonas putida*. *Am. Mineral.* **2006**, *91* (4), 489–502.

(8) Kirillov, S. A.; Aleksandrova, V. S.; Lisnycha, T. V.; Dzanashvili, D. I.; Khainakov, S. A.; García, J. R.; Visloguzova, N. M.; Pendelyuk, O. I. Oxidation of synthetic hausmannite (Mn_3O_4) to manganite (MnOOH). *J. Mol. Struct.* **2009**, *928* (1–3), 89–94.

(9) Hem, J. D.; Roberson, C. E.; Fournier, R. B. Stability of *β*MnOOH and manganese oxide deposition from springwater. *Water Resour. Res.* **1982**, *18* (3), 563–570.

(10) Elzinga, E. J. Reductive transformation of birnessite by aqueous Mn(II). *Environ. Sci. Technol.* **2011**, *45* (15), 6366–6372.

(11) Lefkowitz, J. P.; Rouff, A. A.; Elzinga, E. J. Influence of pH on the reductive transformation of birnessite by aqueous Mn(II). *Environ. Sci. Technol.* **2013**, *47* (18), 10364–10371.